Nanoscale

Electron-Phonon Relaxation at Au/WSe2 Interface is Significantly Accelerated by a Ti Adhesion Layer: Time-Domain Ab Initio Analysis

Journal:	*Nanoscale*
Manuscript ID	NR-ART-02-2022-000728.R1
Article Type:	Paper
Date Submitted by the Author:	16-Jun-2022
Complete List of Authors:	Lu, Teng-Fei; Jilin University, institute of theoretical chemistry; University of Southern California, department of chemistry Gumber, Shriya; University of Southern California, Chemistry Tokina, Marina; University of Southern California, Chemistry Tomko, John; University of Virginia, Mechanical and Aerospace Engineering Hopkins, Patrick E.; Univ Virginia Prezhdo, Oleg; University of Southern California, Chemistry

Electron-Phonon Relaxation at Au/WSe_2 Interface is Significantly Accelerated by a Ti Adhesion Layer: Time-Domain *Ab Initio* Analysis

Teng-Fei Lu[1], Shriya Gumber[2], Marina V. Tokina[2], John A. Tomko,[3] Patrick E. Hopkins,[3,4,5] Oleg V. Prezhdo[2,6*]

[1]*School of Materials Science and Engineering, Dalian Jiaotong University, Dalian 116028, Liaoning Province, China*

[2]*Department of Chemistry, University of Southern California, Los Angeles, CA 90089, USA*

[3]*Department of Mechanical and Aerospace Engineering, University of Virginia, Charlottesville, VA 22904, USA*

[4]*Department of Materials Science and Engineering, University of Virginia, Charlottesville, VA 22904, USA*

[5]*Department of Physics, University of Virginia, Charlottesville, VA 22904, USA*

[6]*Department of Physics and Astronomy, University of Southern California, Los Angeles, CA 90089, USA*

[*] Corresponding author, E-mail: prezhdo@usc.edu

ABSTRACT

Thermal transport at nanoscale metal-semiconductor interfaces via electron-phonon coupling is crucial for applications of modern microelectronic, electro-optic and thermoelectric devices. To enhance the device performance, the heat flow can be regulated by modifying the interfacial atomic interactions. We utilize *ab initio* time-dependent density functional theory combined with non-adiabatic molecular dynamics to study how the hot electron and hole relaxation rates change on incorporating a thin Ti adhesion layer at the Au/WSe_2 interface. The excited charge carrier relaxation is much faster in Au/Ti/WSe_2 due to the enhanced electron-phonon coupling, rationalized by the following reasons: (1) Ti atoms are lighter than Au, W and Se atoms, and move faster. (2) Ti has a significant contribution to the electronic properties at the relevant energy range. (3) Ti interacts strongly with WSe_2 and promotes its bond-scissoring which causes Fermi level pinning, making WSe_2 contribute to electronic properties around the Fermi level. The changes in the relaxation rates are more pronounced for excited electrons compared to holes because both relative and absolute Ti contributions to the electronic properties are larger above than below the Fermi level. The results provide a guidance for improving the design of novel and robust materials by optimizing the heat dissipation at metal-semiconductor interfaces.

1. Introduction

Increasing demand and ongoing trend for versatile, high-speed and high-density electronics is pushing the limits for miniaturization of electronic devices to atomic thickness. As silicon-based devices are approaching their limit to keep up with the Moore's Law, there is a need for an alternate semiconductor material that can continue to shrink the size of electronic devices while maintaining their efficiency. Atomically thin two-dimensional (2D) semiconductors, transition-metal dichalcogenides (TMDs) are potential candidates for silicon replacement in low power devices owing to their stability, long-life and tunable band gap.[1-4] However, the true capability of TMDs is masked by their large contact resistance at interfaces, which necessitates the optimization of such devices to control the interfacial properties.[5]

Thermal resistance at interfaces can inhibit the removal of excess heat that can compromise with reliability and deter the performance of ultrasmall devices.[6] In metals, electrons govern the transfer of energy, while lattice vibrations or phonons are responsible for the heat flow in semiconductors. At interfaces, two phenomena are likely to occur: First, the electrons in metal couple to the phonons in metals and then the phonons in metal transfer energy to the phonons in semiconductor; Second, the electrons in metal couple directly to the phonons in semiconductor. A comprehensive understanding of thermal equilibration of excited electrons with lattice is crucial for various applications.[7] Experimentally, time-resolved pump-probe laser techniques are used to advance the understanding of energy transfer processes occurring over pico- and sub-picoseconds time scales.[8-12] Over the years, a number of theoretical models have been developed to mimic these experimental techniques.[13-16]

The most popular approach, two-temperature model (TTM) considers that the irradiation of a metal surface by ultrashort laser pulse creates thermodynamic non-equilibrium electron

distribution,[17,18] as the optical pulse can only couple directly to electrons; the temperature of the phonon subsystem remains unaffected due to the large difference in the electronic and lattice heat capacities ($C_p \gg C_e$). Over tens or few hundreds of femtoseconds, the electronic subsystem equilibrates to the Fermi-Dirac distribution at a higher temperature through electron-electron scattering. Thereafter, the electrons equilibrated at an elevated temperature redistribute their energy to the phononic subsystem until the two temperatures become equal. The rate of energy transfer depends on the electron-phonon coupling constant G and the temperature differential of the two subsystems.[11] The coupling is thus enhanced under conditions of strong non-equilibrium between the electron and phonon subsystems. The TTM theory was first confirmed experimentally by Eesley, who studied the evolution of non-equilibrium between the electronic and vibrational states using ultrafast pump-probe spectroscopy.[19] Using the TTM, Majumdar and Reddy derived an analytical expression to study how the electron-phonon coupling in metal affects the thermal boundary resistance across metal/non-metal interfaces.[20] Chen et al. proposed improvement to the TTM model by introducing a temperature dependent electron-phonon coupling constant, G_{eff}.[21] However, this method is only valid for materials that have a constant density of states (DOS) over all electron temperature range until the Fermi temperature is reached. Further modifications to this model were introduced by Zhigilei and co-workers.[22] They calculated the electron-phonon coupling constant using electronic structure calculations and studied the temperature dependence of the electron-phonon coupling factor for several different metals accounting for variations in the chemical potential and electron density of states beyond free electron theory as the degree of electron-phonon thermal nonequilibrium increased.

The TTM has been frequently utilized to study numerous bulk systems in the past, however, the assumption of quasi-equilibration of electron energy is troublesome for nano-sized

metallic systems.[23,24] In bulk metals, the electron energy equilibrates due to the Cherenkov generation of acoustic waves. But this mechanism is absent in case of nano-sized metallic systems.[25] For ultrasmall systems, energy carrier dynamics are fast, and the energy distributions are highly out of equilibrium. This inspires the time-domain atomistic simulations in such regimes to mimic the ultrafast laser measurements.

The electron-phonon energy transfer across interfaces is strongly influenced by the interfacial atomic interactions.[26] A transition metal film, usually Ti, is often inserted at the interface to alter the electronic and optical response, as well as increase adhesion of poorly bonded layers.[27-30] Giri et al. demonstrated that on incorporation of thin Ti adhesion layer between Au slab and a non-metal substrate, the electron-phonon coupling is enhanced resulting in accelerated energy relaxation.[31] The increase in energy exchange near the interface is rationalized by the strengthened bonding between Au and non-metal when a Ti layer is included. Zhou et al. used time-domain *ab initio* analysis and observed that the relaxation between electrons and phonons accelerate on placing a Ti adhesion layer on gold films.[32, 33] Freedy et al. utilized time-domain thermo-reflectance to report that the high thermal conductance at Au-Ti-WSe_2-HOPG interfaces is due to strong interaction of Ti adhesion layer with WSe_2 at the interface.[29]

In this paper, we utilize *ab initio* time-dependent density functional theory (TD-DFT) within Kohn-Sham (KS) framework, combined with non-adiabatic (NA) molecular dynamics (MD) to study how thermal relaxation of excited charge carriers at Au/WSe_2 interface is influenced when a Ti adhesion layer is sandwiched between Au and WSe_2 resulting in Au/Ti/WSe_2. Tungsten diselenide (WSe_2) is a 2D transition metal dichalcogenide that consists of a strongly bound Se-W-Se sandwich weakly stacked with other layers by van der Waals interactions.[34-36] For interface, gold (Au) slab is considered because of its simple structure and available literature that makes the

comparative study between experiments and theory convenient.[37] Time-domain NA-MD is efficient to probe the non-equilibrium processes that are critical for a wide-range of applications in nanostructures, semiconductors and at interfaces.[38-50] It mimics the time-resolved pump-probe laser experiments and aids us to gain insight into processes that happen over sub-picoseconds scale.

2. Computational Details and Methodology

A mixed quantum-classical approach is employed to investigate the non-equilibrium dynamics of excited electron relaxation. The electronic evolution is studied quantum mechanically using KS-DFT and the nuclear trajectory is obtained using classical MD. NA-MD is used to model the electron-nuclear interactions.[51-59]

Initially, geometry relaxation, electronic structure and MD calculations are performed using the Vienna *ab initio* simulation package (VASP), which uses plane wave basis sets to describe the periodic structure.[60-62] The Perdew-Burke-Ernzerhof (PBE) generalized gradient DFT functional described the nonlocal exchange and correlations contribution to the electronic energy.[63] The projector-augmented wave (PAW) approach is used to express the interactions between ionic cores and valence electrons.[64] The following VASP pseudopotentials were used: PAW_PBE Au 06Sep2000, PAW_PBE Ti 08Apr2002, PAW_PBE W 08Apr2002 and PAW_PBE Se 06Sep2000. The van der Waals interactions at the interface were described using the DFT-D3 method.[65] The cutoff energy for plane wave basis set was set at 400 eV. The electronic energy and ionic forces were converged to 10^{-6} eV and 0.02 eV/Å, respectively.

The two systems under investigation, Au/WSe_2 and Au/Ti/WSe_2 were set up using the VESTA software.[66] The Au/WSe_2 system is made up of an Au slab cut at the (111) lattice plane, and it has five layers of Au atoms at interface with a monolayer WSe_2. The supercell contains 40

Au, 12 Se and 6 W atoms. Au/Ti/WSe_2 was constructed by placing a Ti (001) monolayer of total 8 atoms sandwiched between the Au slab and the WSe_2 monolayer of same dimensions. To avoid spurious interactions with periodic slabs, a vacuum layer of 20 Å was introduced perpendicular to the surface. The $5 \times 5 \times 1$ Monkhorst-Pack mesh was used for the structural optimization, molecular dynamics and DOS calculations.

After geometry optimization at 0 K, the temperature was raised up to 300 K using repeated velocity rescaling to mimic the experimental conditions. Following thermalization, MD simulations were performed for a total of 4 ps in microcanonical ensemble with a time step of 1 fs. Adiabatic state energies and the NA coupling (NAC) matrix were computed for geometry at every time-step. Total 1000 stochastic surface hopping realizations for each of the 500 geometries sampled from the MD trajectory as initial conditions were used for electron-nuclear evolutions. The 4 ps trajectory was replicated twice to obtain longer time results for NA-MD.

Electronic basis states can be represented in several ways,[67] however, for computational convenience, Slater determinant constructed using KS orbitals is preferred.[68-71] In KS representation of DFT, electron density of a system is used to describe the evolution of all its electronic properties. It is represented by the sum of densities of all occupied single electron KS orbitals:

$$\rho(t) = \sum_{i=1}^{N_e} \left| \widetilde{\Phi}_i(r,t) \right|^2 \quad (1)$$

where N_e is the total number of electrons. The equations-of-motion for the single particle time-dependent KS orbitals is obtained by applying the time-dependent variational principle to the expectation value of the KS density functional,

$$i\hbar \frac{\partial}{\partial t} \Phi_i(r,t;R) = H(r,R,t)\Phi_i(r,t;R) \quad (2)$$

Here, $H(r,R,t)$ is a functional of the total electron density, and hence the equations of each particle are coupled and not independent. The nuclear degrees of freedom are treated parametrically and they evolve on the respective adiabatic state using quantum force e.g., the Hellmann-Feynman force. The time-dependent KS orbitals can be expanded in terms of the adiabatic KS orbital basis, computed for a given nuclear configuration, R(t), using the time-dependent coefficients,

$$\Phi_i(r,t) = \sum_{k=1}^{N_e} c_{ik}(t)\left|\widetilde{\Phi}_k(r;R)\right\rangle \quad (3)$$

Combining eqs. (2) and (3) produces equation-of-motion for the expansion coefficients:

$$i\hbar\frac{\partial c_{ij}(t)}{\partial t} = \sum_{k=1}^{N_e} c_{ik}(t)(\varepsilon_k\delta_{jk} + d_{jk}.\dot{R}) \quad (4)$$

Here ε_k is the energy of k^{th} adiabatic KS orbital, and d_{jk} is the NAC vector between adiabatic states j and k. The coupling arises from the dependence of adiabatic electronic states on the nuclear trajectory. The dot product of the NAC with the nuclear velocity is numerically calculated by taking the overlap of the adiabatic wavefunctions of the two states at sequential time-steps.[72, 73]

$$d_{jk}.\dot{R} = -i\hbar\left\langle\widetilde{\Phi}_j\left|\nabla_R\right|\widetilde{\Phi}_k\right\rangle.\frac{dR}{dt} = -i\hbar\left\langle\widetilde{\Phi}_j\left|\frac{\partial}{\partial t}\right|\widetilde{\Phi}_k\right\rangle \quad (5)$$

To model the excited electron relaxation dynamics, a method that can efficiently describe the transitions between electronic states is desired. For the work in this paper, we use the global flux surface hopping (GFSH) method.[74,75] within the classical path approximation as implemented in the PYXAID program.[68, 69] GFSH is a generalization of fewest switches surface hopping,[76, 77] which is the standard method for modelling electron-phonon relaxation dynamics in condensed matter. The probability of electronic transitions between electronic states is calculated using the solution of time-dependent Schrodinger equation.

$$dP_{jk} = \left(-\frac{2Re\left(\alpha_{jk}^{*}d_{jk}\dot{R}\right)}{\alpha_{jj}}\right)dt \quad (6)$$

where $\alpha_{jk} = c_j^* c_k$. j and k are the electronic states under consideration and dt is the time interval. If dP_{jk} is negative, the transition probability is set to zero. To determine if transition to a state will happen, the probability of transition is compared to a random number uniformly generated between 0 to 1 at every time step. The detailed balance between transitions upward and downward in energy is achieved by accepting transitions upward in energy with the Boltzmann probability, reflecting the probability that sufficient kinetic energy is present in the motion along the direction of the NAC that induces the transition.

3. Results and Discussion

On geometry relaxation of both systems under investigation, Au/WSe_2 and Au/Ti/WSe_2, the structural integrity of all materials in the supercell is preserved. WSe_2 displays a small-scale sliding on incorporation of the Ti adhesion layer between the Au slab and the WSe_2 monolayer, Figure 1. The distance between WSe_2 and the nearest Au layer in Au/WSe_2 is 2.807 Å, while the nearest Au layer-Ti layer and Ti layer-WSe_2 distances in Au/Ti/WSe_2 are maintained at 2.236 Å and 2.265 Å, respectively. The average Au-Ti distance is similar to that observed and calculated in the Au/Ti interfacial system in the absence of WSe_2 monolayer indicating that WSe_2 has little influence on the interaction between Au and Ti. The two Se layers in WSe_2 are in different environments altogether. The W-Se distance for Se which is in direct contact with the Au slab in Au/WSe_2 and the Ti layer in Au/Ti/WSe_2, is termed as “Se-con”, while the W-Se distance for which Se is not in direct contact to any other element is called “Se-non”, Figure 1.

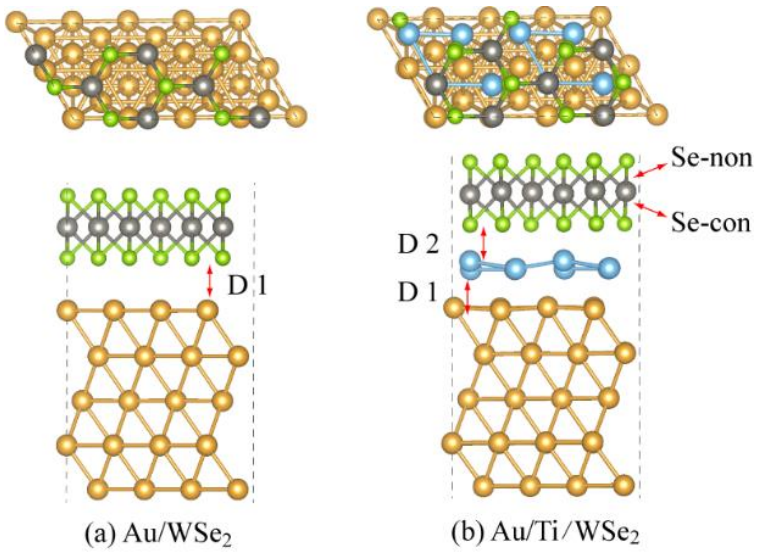

Figure 1. Top and side views of the simulation cell showing **(a)** Au/WSe_2 and **(b)** Au/Ti/WSe_2. "D 1" indicates the interface distance between WSe_2 or Ti layer in contact with Au. "D 2" indicates the interface distance between WSe_2 and Ti. "Se-con" and "Se-non" indicate Se atoms in direct contact and not in direct with the Ti metal, respectively.

The thermal effects when the temperature is raised up to 300 K and the inclusion of the Ti adhesion layer between the Au slab and the WSe_2 monolayer have notable impacts on the geometry and interlayer distance of all materials in the system, as evident from data in Table 1. On heating, the system expands, and as a result, the average inter-layer distance increases by ~ 0.027 Å for both Au-WSe_2 and Au-Ti. However, there is no significant change in the Ti-WSe_2 (0.003 Å). In Au/WSe_2, the average W-Se bond length at 300 K is exactly equal to the bond length at 0 K, however, in case of Au/Ti/WSe_2, the W-Se bond length elongates by 0.002-0.003 Å. Titanium interacts with WSe_2 and lengthens the W-Se-con bond distance (2.588 Å), indicating that Ti leads to bond scissoring in WSe_2, which results in increased elemental W and bonded Ti-Se characters. Overall, the influence of the Ti-WSe_2 interactions on the system geometry is much stronger than the thermal effects, Table 1.

Table 1 : Calculated Average W-Se Bond Length, Average Ti-Se Bond Length, Interface Distance Between Au and either WSe_2 or Ti (D 1), Figure 1, and Interface Distance Between WSe_2 and Ti (D 2) at 0 K and 300 K.

		Average W-Se Bond Length		Average Ti-Se Bond Length		D 1		D 2	
		0 K	300 K	0 K	300 K	0 K	300 K	0 K	300 K
Normal		2.548 Å	2.548 Å						
Au/WSe_2		2.544 Å	2.544 Å			2.807 Å	2.834 Å		
Au/Ti/WSe_2	**Se-con**	2.588 Å	2.592 Å	2.517 Å	2.520 Å	2.236 Å	2.254 Å	2.265 Å	2.268 Å
	Se-non	2.539 Å	2.541 Å						

To characterize the electronic structure, the projected density of states (PDOS) of the optimized geometry is computed as shown in Figure 2a. The PDOS is derived by separation of total density of states into contributions from Au (red), Ti (green) and WSe_2 (blue). The Fermi level is set to zero. There is no band gap in the DOS of Au as a result of its metallic character. In the Au/WSe_2 system, the most striking observation is that the Au DOS undergoes a sharp fall in the energy range from -2 eV to -1 eV. The electronic states at energies below the sharp fall are formed by *d* orbitals of Au atoms, while *d* orbitals do not contribute to the higher energy states, which are formed predominantly from *p* orbitals of Au. In the energy range from -7 eV to -1.5 eV both Au and WeS_2 contribute to the DOS, however, Au dominates. The band gap of WSe_2 lies in the energy range from -0.7 to 0.4 eV. The DOS at and near the Fermi energy is small, since it resides within the WSe_2 band gap, and the Au DOS has experienced the large drop below the Fermi level. WeS_2 dominates the DOS at energies above 1 eV. Due to large DOS below -2 eV relaxation of deep holes should be significantly faster than relaxation of shallow holes.

In case of Au/Ti/WSe_2, no significant changes occur in the DOS contribution from Au, however, the WSe_2 DOS is significantly altered, Figure 2b. The band gap of WSe_2 is critically

determined by the W-Se covalent bonding, and the band-edges is mainly constituted of W d-orbitals. The Ti metal contact disturbs the electron distribution surrounding Se-con atoms. Consequently, W-Se-con bonding is affected resulting in production of gap states. The interfacial strong Ti-Se bonding weakens the intralayer W-Se-con bonding, and thus the W d-states at the band edges spread into the band gap, producing gap states. WSe_2 character changes to metal-like with almost negligible band gap. The process of introducing new electronic states into the band gap because of interfacial reaction products is called Fermi-level pinning.[64] Moreover, the Ti metal has maximum DOS contribution starting from -1.5 eV to higher energy states. It has negligible contribution until -1.5 eV, and hence the modification in the DOS caused by the Ti adhesion layer is more significant above the Fermi level. In the energy range from -1.5 eV to 0 eV Au and Ti have almost equal contributions to the DOS. This is quite remarkable, since the system contains five times more Au atoms than Ti atoms. In the energy range from 0 to 3.1 eV, the contribution of Ti and WSe_2 is more significant than the contribution of Au. Considering that Ti atoms constitute only 1/8 of all atoms, we conclude that the Ti adhesion layer significantly influences the electronic states in the relevant energy region.

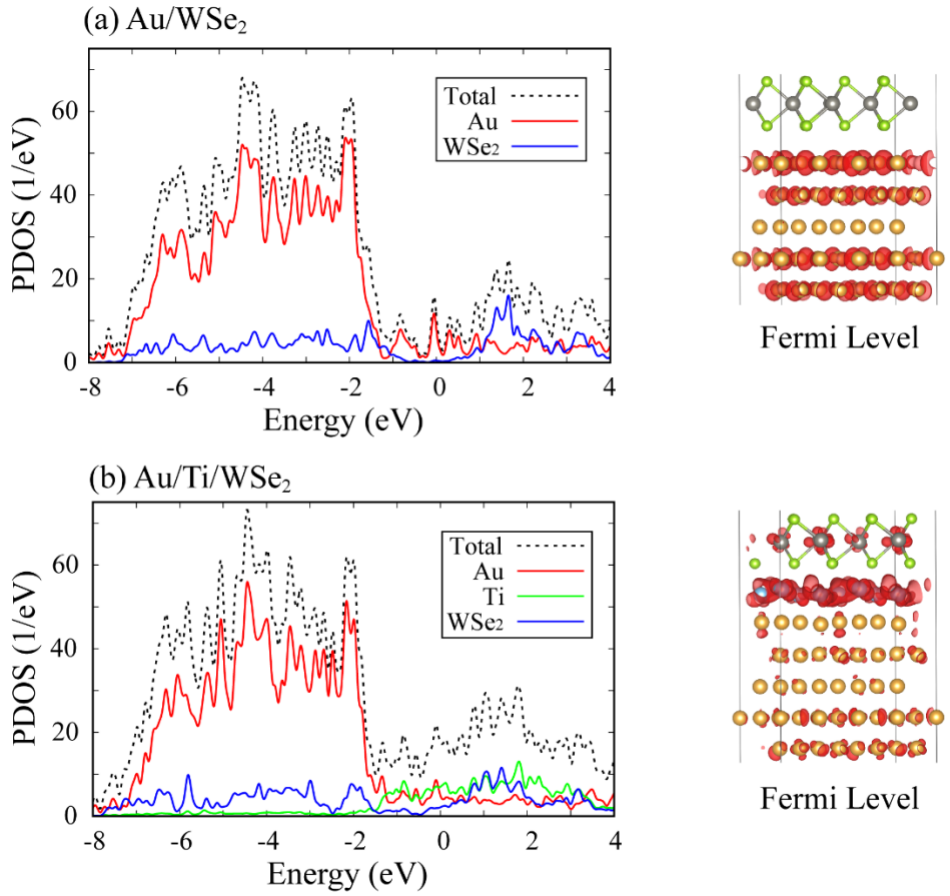

Figure 2. Projected density of states (PDOS) in the left panel and charge densities of the Fermi level in the right panel of **(a)** Au/WSe_2 and **(b)** $Au/Ti/WSe_2$.

The right panels of Figure 2 show charge densities of the electronic states at the Fermi level for both systems under consideration. In case of Au/WSe_2, the density of the Fermi level is completely localized on Au, and there is no contribution from WSe_2. As understood from PDOS, the band gap of WSe_2 encompasses the Fermi level, and hence WSe_2 does not contribute to the charge density. In the case of $Au/Ti/WSe_2$, the charge density is delocalized on the whole system, while it is most dense at Ti, indicating that Ti supports the most mobile electrons in the system. Further, the Fermi level charge density of $Au/Ti/WSe_2$ shows contributions from W, reflecting the increased DOS of WSe_2 near the Fermi energy, resulting from WSe_2 distortion due to interaction with Ti and the Fermi level pinning. The charge density contribution by Au is sparse and less

dense, compared to contributions from Ti and W, as well as the charge density of Au in Au/WSe_2 at the Fermi level.

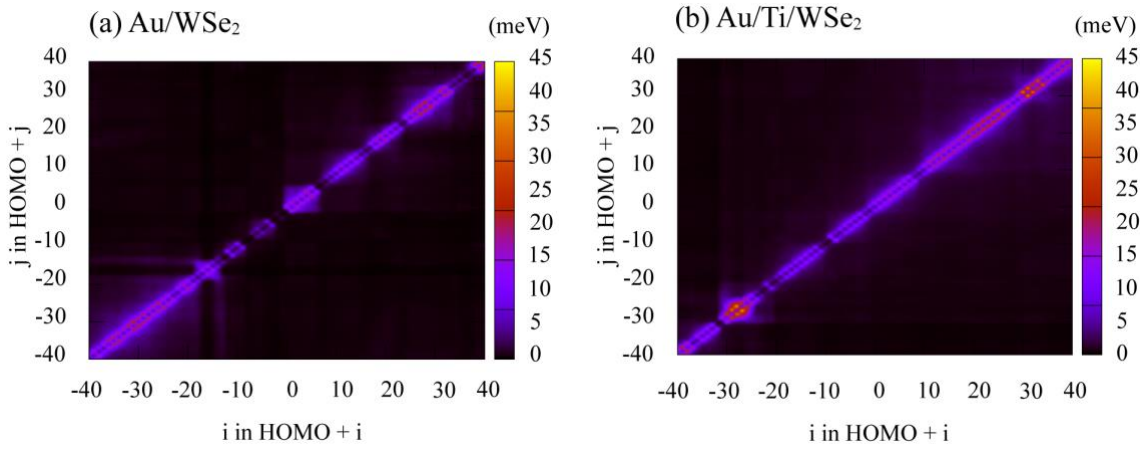

Figure 3. Visualization of the averaged absolute nonadiabatic couplings between states labeled by orbital indices for **(a)** Au/WSe_2 and **(b)** Au/Ti/WSe_2.

Electron and phonon subsystems interact leading to elastic and inelastic electron-phonon scattering. Elastic scattering results in dephasing of the electronic states by randomization of the phase of the electronic wavefunction, and it is measured by the pure-dephasing time.[78-80] Inelastic scattering leads to energy exchange between the electrons and phonons, and it is characterized by the NAC. Here, we focus on the electron-phonon energy exchange. The coupling strength between two electronic states is directly related to localization of the wavefunction of the corresponding electronic states, see Eq. (5). The magnitude of NAC determines the frequency and time-scale of NA transitions between the electronic energy levels. In surface hopping, a sequence of NA transitions governs the electron-phonon relaxation rate. Figure 3 shows the phonon-induced NAC of both systems for ±50 electronic states around the Fermi energy, i.e., the highest occupied molecular orbital (HOMO). As expected, both the plots are diagonally symmetric confirming that the magnitude of state i coupling to j or state j coupling to i is equal. The diagonal data points (black) have zero NAC magnitude because the electronic states do not couple to themselves. The

brighter purple-red traces in the plot corresponds to the coupling between consecutive electronic states. The rest of the non-diagonal part represents the electronic states that differ by two or more. The NAC between distant states is much weaker than the coupling between neighbor states, indicating that the electron-phonon energy relaxation occurs by small energy transitions, and that large energy hops are possible occasionally.

The NAC strength is much larger in Au/Ti/WSe_2 compared to Au/WSe_2 throughout the plot, Figure 3. In presence of the Ti adhesion layer, the DOS is relatively dense around the Fermi level, and the coupling strength is generally higher for states closer in energy. Ti is the dominant element contributing to the electronic states in the corresponding energy region. Further, Eq. (5) shows that the NAC is directly related to the nuclear velocities, and nuclear velocities are inversely proportional to the square root of the atomic mass, at a given temperature. Ti is four times lighter than Au, and hence the velocity difference increases the NAC by a factor of two. W is nearly as heavy as Au. Se is twice heavier than Ti, however, it has no contribution near the Fermi energy and contributes little to the WSe_2 conduction band. Se contributes to the $WeSe_2$ valence band, however, the DOS in that energy region is strongly dominated by Au, Figure 2. Overall, the NAC strength is expected to be larger in region where Ti electronic states are dominant. Consequently, the influence of the Ti adhesion layer should be more significant above the Fermi energy.

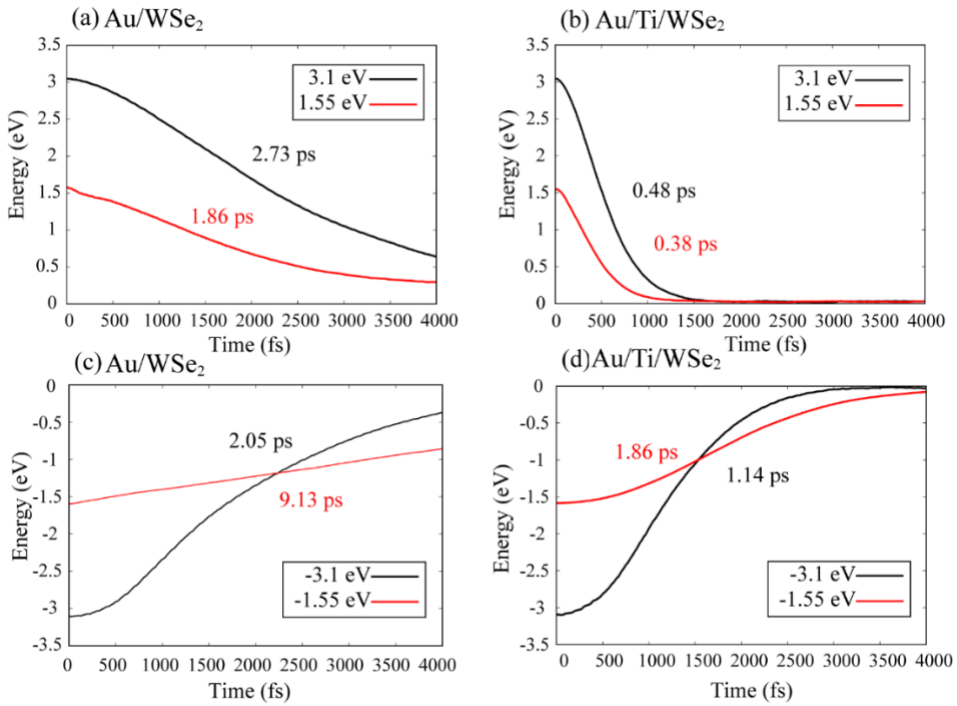

Figure 4. Evolution of electron (**a** and **b**) and hole (**c** and **d**) energy starting from high (3.1 eV) and low (1.55 eV) energy initial states in (**a** and **c**) Au/WSe_2 and (**b** and **d**) $Au/Ti/WSe_2$.

The photoexcited charge carriers dissipate their energy by coupling to phonons. The rate of relaxation through manifold of states depends on the strength of respective NAC, Figure 3. Figure 4 shows the evolution of the average energy of the charge carriers in the two systems beginning at high and low energy initial conditions: 3.1 and 1.55 eV in case of electrons, and -3.1 and -1.55 eV in case of holes. The initial conditions are chosen to match the experiments.[28,29] The electronic subsystem is pumped at 400 nm, corresponding to ~3.1 eV. The 3.1 eV of energy is distributed between electron and hole. The initial conditions represent two limiting cases. Either half of the energy is given to the electron and half to the hole, resulting in 1.55 eV excitation of each, or all energy is given to either electron or hole. Because the dense *d*-band of Au starts about 1.7 eV below the Fermi level, as seen in the rapidly rising DOS in Figure 2, majority of the carriers are excited from around this energy, and the symmetrical initial condition provides a better representation of the experiments.[28,29]

As expected for all quantum dynamical systems, the dynamics is Gaussian in the beginning. The exponential regime, associated with participation of many states, is achieved relatively fast. The Gaussian regime of quantum dynamics gives rise to the Zeno effect, in which continuous measurement of the quantum system effectively slows down the dynamics.[81] The measurement in the current process is associated with electronic wavefunction dephasing due to elastic electron-phonon scattering. Because the relaxation occurs through dense manifolds of electronic states, the elastic pure-dephasing process is slow relative to the frequency of inelastic quantum transitions. The Fermi energy level is set to zero in Figure 4, and the decay time are obtained by fitting the data to an exponential function, $Aexp\ (-t/\tau)$. While no experimental time-traces are available in literature for the systems under investigation, time-resolved data are available for systems composed of Au films on other semiconductor substrates, including Si, SiO_2, TiO_2 and Al_2O_3 with and without Ti adhesion layers.[31,82,83] The measured timescales are similar to those obtained in the present calculations.

In case of Au/WSe_2, there is a steep decrease in the electronic DOS above -1.5 eV, Figure 2. Consequently, the decay of holes starting from -1.5 eV is much slower than the decay of holes beginning at -3.1 eV, Figure 4c. The frequency of transitions is slow in the region where electronic states are sparse. Moreover, it is slower when electronic states are contributed by Au compared to Ti due to Au heavier mass, slower velocity, and smaller NAC, Eq. (5). Therefore, on addition of Ti, the involvement of Ti states post -1.5 eV substantially increases the relaxation rate of holes, Figure 4d. Overall, the relaxation of holes is faster in the presence of Ti. Similarly, the hot electron decay is faster in Au/Ti/WSe_2 compared to Au/WSe_2, Figure 4a,b, while the timescales of electron decay beginning at different energy levels are comparable within each system due to homogeneous DOS above the Fermi level, Figure 2. Notably, the influence of the Ti adhesion layer is more

pronounced for relaxation of hot electrons compared to holes. This can be rationalized by the more significant Ti contribution to the DOS above the Fermi level in Figure 2b.

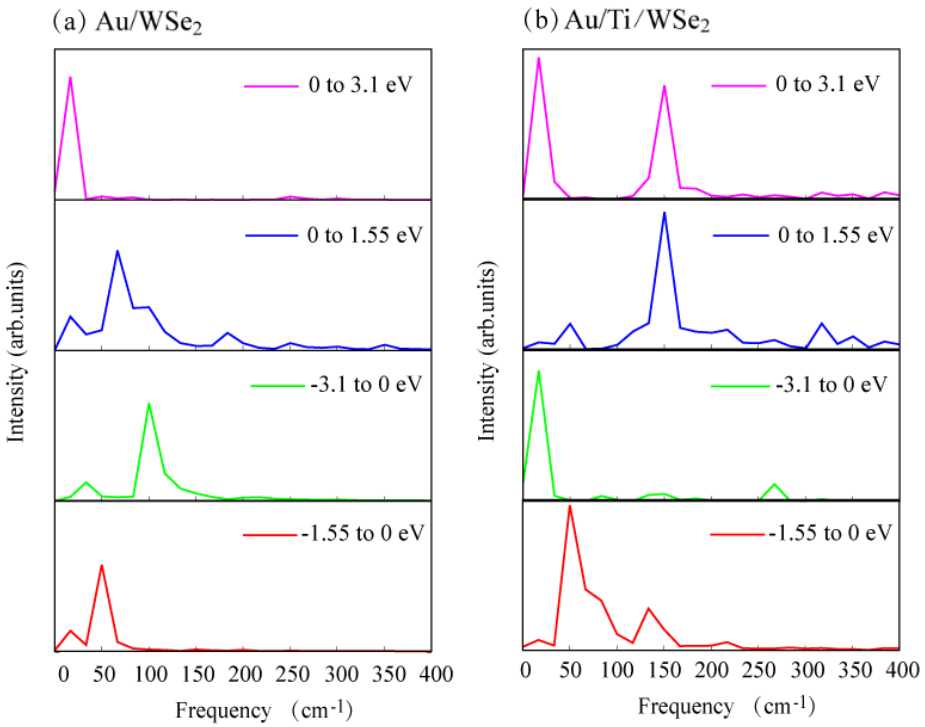

Figure 5. Phonon influence spectra for the energy gaps from the Fermi level to the high or low energy initial states for the electron relaxation (top two panels) and hole relaxation (bottom two panels) in **(a)** Au/WSe_2 and **(b)** $Au/Ti/WSe_2$

To further advance the understanding of the electron-phonon scattering, we obtain the phonon influence spectra. It helps to identify the frequencies of the phonon modes that couple to the electronic subsystem and dissipate the electronic energy.[66] The phonon influence spectra are obtained by computing the Fourier transform of the autocorrelation functions of the energy gaps between the initial and final states in each simulation, i.e., between the hole energy level at -3.1 eV and the Fermi level (HOMO) at 0 eV, the hole energy level at -1.55 eV and the Fermi level at 0 eV, the electron energy level at 3.1 eV and the Fermi level, and the electron energy level at 1.55 eV and the Fermi level. This particular choice is made for representative purposes, since around

50 states are involved in the studied NA dynamics of both electrons and holes, and the number of energy gaps is on the order of 1000. The height of the peaks in Figure 5 indicates the strength of the electron-phonon coupling at the corresponding frequency.

The influence spectra show only very weak signals at frequencies above 200 cm^{-1}. The Ti adhesion layer introduces higher frequency phonons, because Ti is lighter than any atom of the Au/WSe_2 system. Moreover, the electron-phonon coupling strength increases as evident from the larger peak heights. Note that while the peak intensity scale is arbitrary, it is consistent across all plots. The influence spectrum characterizing holes starting at -3.1 eV exhibits a strong peak at 100 cm^{-1}, which is not seen for the -1.5 eV signal, compare the third and bottom panels in Figure 5a. This is because Se atoms are lighter than both Au and W, and contribute to the valence band states of WSe_2, which participates in the relaxation of deep holes. The Ti peaks at 150 cm^{-1} are stronger for electrons than holes, compare the top two and bottom two panels in Figure 5b. This is because Ti has a much larger absolute and relative contribution to the DOS above than below the Fermi energy, Figure 2. We conclude that the photogenerated charges always couple to phonons in the metal, and the Ti adhesion layer makes this coupling stronger. The phonons of the WSe_2 semiconductor couple to the excited charges only when the energy of the charges is within the range of the conduction or valence band of WSe_2.

4. Conclusion

We performed *ab initio* quantum dynamics simulations to model two related systems: Au/WSe_2 and Au/Ti/WSe_2, and thus study the effect of a thin Ti adhesion layer on excited electron and hole relaxation dynamics at the interface between Au and WSe_2. Related metal-semiconductor interfaces are ubiquitous in electro-optical devices, and it is essential to optimize such devices to

minimize the thermal resistance at the interfaces. It was observed that inclusion of Ti at the interface increases the strength of the electron-phonon coupling and hence accelerates the relaxation dynamics. We thoroughly investigated the reasons behind the enhanced coupling strength. Because Au has low DOS around the Fermi level, which falls within the WSe_2 band gap, even a thin Ti adhesion layer has a strong influence on the electronic properties and electron-phonon coupling at the relevant energy range. The Ti adhesion layer makes a significant direct contribution to the electronic DOS. In addition, Ti interacts strongly with WSe_2 to elevate the W metallic character and Ti-Se bonding, while weakening W-Se bonding. This results in the Fermi level pinning, increasing WSe_2 contribution to the electronic states in the relevant energy window. Further, Ti atoms are lighter by a factor of four than Au and W atoms, and by a factor of two than Se atoms. Consequently, Ti atoms move faster and accelerate the electron-vibrational energy exchange. Se atoms contribute to the DOS where it is dominated by Au, and therefore, the contribution of Se to electron-phonon relaxation is less important compared to the Ti, Au and W metal atoms. By increasing the DOS and moving fast, Ti atoms increase the NAC and accelerate the charge-phonon relaxation. Because Ti has a more significant contribution to the electronic properties above than below the Fermi energy, the electron relaxation is accelerated more than the hole relaxation. These results can be used for designing modern electronic devices by altering thermal conductance at metal-semiconductor interfaces.

Conflicts of interest

There are no conflicts of interest to declare.

Acknowledgements

The research was supported by the US Department of Defense, Multidisciplinary University Research Initiative, grant No. W911NF-16-1-0406, and the Semiconductor Research Corporation, Award Number 2021-NM-3047.

References:

(1) S. Manzeli, D. Ovchinnikov, D. Pasquier, O. V. Yazyev and A. Kis, *Nature reviews Materials,* 2017, **2**, 17033. DOI: 10.1038/natrevmats.2017.33.
(2) C. N. R. Rao, U. Maitra and U. V. Waghmare, *Chemical Physics Letters,* 2014, **609**, 172-183. DOI: 10.1016/j.cplett.2014.06.003.
(3) R. Nur, T. Tsuchiya, K. Toprasertpong, K. Terabe, S. Takagi and M. Takenaka, *Nanoscale,* 2022, DOI: 10.1039/D1NR06315D.
(4) H. Jin, T. Wang, Z.-R. Gong, C. Long and Y. Dai, *Nanoscale,* 2018, **10**, 19310. DOI: 10.1039/C8NR04568B.
(5) Y. Liu, Z.-Y. Ong, J. Wu, Y. Zhao, K. Watanabe, T. Taniguchi, D. Chi, G. Zhang, J. T. L. Thong, C.-W. Qiu and K. Hippalgaonkar, *Scientific reports,* 2017, **7**, 1-8. DOI: 10.1038/srep43886.
(6) E. Pop, *Nano Res,* 2010, **3**, 147-169. DOI: 10.1007/s12274-010-1019-z.
(7) H.E. Elsayed-Ali, T. B. Norris, M. A. Pessot and G. A. Mourou, *Phys. Rev. Lett.,* 1987, **48**, 1212-1215. DOI: 10.1103/PhysRevLett.58.1212.
(8) H. E. Elsayed-Ali, T. B. Norris, M. A. Pessot and G. A. Mourou, *Phys. Rev. Lett.,* 1987, **48**, 1212-1215. DOI: 10.1103/PhysRevLett.58.1212.
(9) B. Y. Mueller and B. Rethfeld, *Appl. Surf. Sci.,* 2014, **302**, 24-28. DOI: 101016/japsusc201312074.
(10) E.M. Grumstrup, M. M. Gabriel, E. M. Cating, C. W. Pinion, J. D. Christesen, J. R. Kirschbrown, E. L. Vallorz, J. F. Cahoon and J. M. Papanikolas, *J. Phys. Chem. C,* 2014, **118**, 8634-8640. DOI: 10.1021/jp502737e.
(11) P. E. Hopkins, L. M. Phinney and J. R. Serrano, *J. Heat Transfer,* 2011, **133**, 044505. DOI: 10.1115/1.4002778.
(12) M. M. Elshanawany, A. G. Ricciardulli, M. Saliba, J. Wachtveitl and M. Braun, *Nanoscale,* 2021, **13**, 15668. DOI: 10.1039/D1NR04290D.
(13) K.-H. Lin and A. Strachan, *J. Chem. Phys.,* 2015, **143**, 034703. DOI: 10.1063/1.4922893.
(14) L. Zhang, J.-T. Lü, J.-S. Wang and B. Li, *J. Phys.: Condens. Matter,* 2013, **25**, 445801. DOI: 10.1088/0953-8984/25/44/445801.
(15) B. Saha, G. Naik, V. P. Drachev, A. Boltasseva, E. E. Marinero and T. D. Sands, *Journal of Applied Physics,* 2013, **114**, 063519. DOI: 10.1063/1.4817715.
(16) Y. Wang, X. Ruan and A. K. Roy, *Phys. Rev. B,* 2012, **85**, 205311. DOI: 10.1103/PhysRevB.85.205311.
(17) S. I. Anisimov, B. L. Kapeliovich, T. L. Perelman, *Journal of Experimental and Theoretical Physics,* 1974, **66**, 776-781. DOI: https://ui.adsabs.harvard.edu/abs/1974ZhETF..66..776A.
(18) T. Q. Qiu and C. L. Tien, *Journal of Heat Transfer,* 1993, **115**, 835-841. DOI: 10.1115/1.2911377.
(19) G. L. Eesley, *Phys. Rev. B,* 1986, **33**, 2144-2151. DOI: 10.1103/PhysRevB.33.2144.
(20) A. Majumdar and P. Reddy, *Appl. Phys. Lett.,* 2004, **84**, 4768-4770. DOI: 10.1063/1.1758301.

(21) J. K. Chen, W. P. Latham and J. E. Beraun, *J. Laser Appl.,* 2005, **17**, 63-68. DOI: 10.2351/1.1848522
(22) Z. Lin, L. V. Zhigilei and V. Celli, *Phys. Rev. B,* 2008, **77**, 075133. DOI: 10.1103/PhysRevB.77.075133.
(23) T. Avanesian and P. Christopher, *J. Phys. Chem. C,* 2014, **118**, 28017-28031. DOI: 10.1021/jp509555m.
(24) N. Singh, *Int. J. Mod. Phys. B,* 2010, **24**, 1141-1158. DOI: 10.1142/S0217979210055366.
(25) E. D. Belotskii and P. M. Tomchuk, *International Journal of Electronics,* 1990, **69**, 169-171. DOI: 10.1080/00207219008920303.
(26) Q. Yao, L. Guo, V. Iyer and X. Xu, *Heat Transfer Eng.,* 2019, **40**, 13-14. DOI: 10.1080/01457632.2018.1457281.
(27) Y.-S. Wang, X. Zhou, J. A. Tomko, A. Giri, P. E. Hopkins and O. V. Prezhdo, *J. Phys. Chem. C,* 2019, **123**, 22842-22850. DOI: 10.1021/acs.jpcc.9b06914.
(28) K. M. Freedy, T. Zhu, D. H. Olson, P. M. Litwin, P. E. Hopkins, M. Zebarjadi and S. J. McDonnell, *2D Materials,* 2020, **7**, 045033. DOI: 10.1088/2053-1583/ab834b.
(29) K. M. Freedy, D. H. Olson, P. E. Hopkins and S. J. McDonnell, *Phys. Rev. Materials*, 2019, **3**, 104001. DOI: 10.1103/PhysRevMaterials.3.104001.
(30) M. Jeong, J. P. Freedman, H. J. Liang, C. Chow, V. M. Sokalski, J. A. Bain and J. A. Malen, *Physical review applied,* 2016, DOI: 10.1103/PhysRevApplied.5.014009.
(31) A. Giri, J. T. Gaskins, B. F. Donovan, C. Szwejkowski, R. J. Warzoha, M. A. Rodriguez, J. Ihlefeld and P. E. Hopkins, *J. Appl. Phys.*, 2015, **117**, 105105. DOI: 10.1063/1.4914867.
(32) X. Zhou, J. Jankowska, L. Li, A. Giri, P. E. Hopkins and O. V. Prezhdo, *ACS Appl. Mater. Interfaces,* 2017, **9**, 43343-43351. DOI: 10.1021/acsami.7b12535.
(33) X. Zhou, L. Li, H. Dong, A. Giri, P. E. Hopkins and O. V. Prezhdo, *J. Phys. Chem. C,* 2017, **121**, 17488-17497. DOI: 10.1021/acs.jpcc.7b05211.
(34) D. J. Late, S. N. Shirodkar, U. V. Waghmare, V. P. Dravid and C. N. R. Rao, *ChemPhysChem,* 2014, **15**, 1592-1598. DOI: 10.1002/cphc.201400020.
(35) Z. Zhou, Y. Zhang, X. Zhang, X. Niu, G. Wu and J. Wang, *J. Mater. Chem. A,* 2020, **8**, 20621. DOI: 10.1039/D0TA06626E.
(36) J. Huang, L. Yang, D. Liu, J. Chen, Q. Fu, Y. Xiong, F. Lin and B. Xiang, *Nanoscale,* 2015, **7**, 4193. DOI: 10.1039/C4NR07045C.
(37) C. M. Smyth, R. Addou, S. McDonnell, C. L. Hinkle and R. M. Wallace, *2D Materials,* 2017, **4**, 025084. DOI: 10.1088/2053-1583/aa6bea.
(38) S. Agrawal, W. Lin, O. V. Prezhdo and D. J. Trivedi, *J. Chem. Phys.,* 2020, **153**, 054701. DOI: 10.1063/5.0010628.
(39) W. Li, A. S. Vasenko, J. Tang and O. V. Prezhdo, *J. Phys. Chem. Lett.,* 2019, **10**, 6219-6226. DOI: 10.1021/acs.jpclett.9b02553.
(40) W. Chu, W. A. Saidi, J. Zhao and O. V. Prezhdo, *Angew. Chem. Int. Ed.,* 2020, **59**, 6435-6441. DOI: 10.1002/anie.201915702.
(41) A. V. Akimov, R. Asahi, R. Jinnouchi and O. V. Prezhdo, *J. Am. Chem. Soc.,* 2015, **137**, 11517-11525. DOI: 10.1021/jacs.5b07454.
(42) L. Li, R. Long, T. Bertolini and O. V. Prezhdo, *Nano Lett.,* 2017, **17**, 7962-7967. DOI: 10.1021/acs.nanolett.7b04374.
(43) W. Li, Y.-Y. Sun, L. Li, Z. Zhou, J. Tang and O. V. Prezhdo, *J. Am. Chem. Soc.,* 2018, **140**, 15753-15763. DOI: 10.1021/jacs.8b08448.
(44) W. Stier, W. R. Duncan and O. V. Prezhdo, *Advanced Materials,* 2004, **16**, 240-244. DOI: 10.1002/adma.200306027.
(45) Z. Zhou, J. Liu, R. Long, L. Li, L. Guo and O. V. Prezhdo, *J. Am. Chem. Soc.,* 2017, **139**, 6707-6717. DOI: 10.1021/jacs.7b02121
(46) C. Cheng, W.-H. Fang, R. Long and O. V. Prezhdo, *JACS Au,* 2021, **1**, 550-559. DOI: 10.1021/jacsau.1c00004.

(47) W. Li, Y. She, A. S. Vasenko and O. V. Prezhdo, *Nanoscale,* 2021, **13**, 10239-10265. DOI: 10.1039/D1NR01990B.
(48) R. Sarkar, M. Habib, S. Pal and O. V. Prezhdo, *Nanoscale*, 2018, **10**, 12683-12694. DOI: 10.1039/C8NR02544D
(49) X. Niu, G. Wu, X. Zhang and J. Wang, *Nanoscale*, 2020, **12**, 6057-6063. DOI: 10.1039/D0NR00447B
(50) X. Niu, Y. Yi, X. Bai, J. Zhang, Z. Zhou, L. Chu, J. Yang and X. Li, *Nanoscale,* 2019, **11**, 4101-4107. DOI: 10.1039/C8NR10142F
(51) J. C. Tully, *J. Chem. Phys.,* 2012, **137**, 22A301. DOI: 10.1063/1.4757762.
(52) J. Jankowska and A. L. Sobolewski, *Molecules,* 2021, **26**, 5140. DOI: 10.3390/molecules26175140.
(53) M. Nottoli, L. Cupellini, F. Lipparini, G. Granucci and B. Mennucci, *Annu. Rev. Phys. Chem.,* 2021, **72**, 489-513. DOI: 10.1146/annurev-physchem-090419-104031.
(54) Z. Tao, Q. Yu, S. Roy and S. Hammes-Schiffer, *Acc. Chem. Res.,* 2021, **54**, 4131-4141. DOI: 10.1021/acs.accounts.1c00516.
(55) M. Barbatti, *WIREs Computational Molecular Science,* 2011, **1**, 620-633. DOI: 10.1002/wcms.64.
(56) M. Ben-Nun, J. Quenneville and T. J. Martínez, *J. Phys. Chem. A,* 2000, **104**, 5161-5175. DOI: 10.1021/jp994174i.
(57) W. H. Miller, *J. Phys. Chem. A,* 2001, **105**, 2942-2955. DOI: 10.1021/jp003712k.
(58) G. A. Worth and L. S. Cederbaum, *Annu. Rev. Phys. Chem.,* 2004, **55**, 127-158. DOI: 10.1146/annurev.physchem.55.091602.09433.
(59) L. Wang, A. Akimov and O. V. Prezhdo, *J. Phys. Chem. Lett.,* 2016, **7**, 2100-2112. DOI: 10.1021/acs.jpclett.6b00710.
(60) G. Kresse and J. Furthmüller, *Phys. Rev. B,* 1996, **54**, 11169-11186. DOI: 10.1103/PhysRevB.54.11169.
(61) G. Kresse and J. Hafner, *Phys. Rev. B,* 1993, **47**, 558-561. DOI: 10.1103/PhysRevB.47.558.
(62) G. Kresse and J. Hafner, *Phys. Rev. B,* 1994, **49**, 14251-14269. DOI: 10.1103/PhysRevB.49.14251.
(63) J. P. Perdew, K. Burke and M. Ernzerhof, *Phys. Rev. Lett.,* 1996, 77, 3865-3868. DOI: 10.1103/PhysRevLett.77.3865.
(64) G. Kresse, D. Joubert, *Phys. Rev. B,* 1999, 59, 1758-1775. DOI: 10.1103/PhysRevB.59.1758.
(65) S. Grimme, J. Antony, S. Ehrlich and H. Krieg, *J. Chem. Phys.,* 2010, **132**, 154104. DOI: 10.1063/1.3382344.
(66) K. Momma and F. Izumi, *J. Appl. Cryst.,* 2011, **44**, 1272-1276. DOI: 10.1107/S0021889811038970.
(67) X. Jiang, Q. Zheng, Z. Lan, W. A. Saidi, X. Ren and J. Zhao, *Science Advances,* 2021, **7**. DOI: 10.1126/sciadv.abf3759.
(68) A. V. Akimov and O. V. Prezhdo, *J. Chem. Theory Comput.,* 2013, **9**, 4959-4972. DOI: 10.1021/ct400641n.
(69) A. V. Akimov and O. V. Prezhdo, *J. Chem. Theory Comput.,* 2014, **10**, 789-804. DOI: 10.1021/ct400934c.
(70) C. F. Craig, W. R. Duncan, O. V. Prezhdo, *Phys. Rev. Lett.,* 2005, **95**, 163001. DOI: 10.1103/PhysRevLett.95.163001.
(71) G. Zhou, G. Lu and O. V. Prezhdo, *Nano Lett.,* 2021, **21**, 756-761. DOI: 10.1021/acs.nanolett.0c04442.
(72) W. Chu and O. V. Prezhdo, *J. Phys. Chem. Lett.,* 2021, **12**, 3082-3089. DOI: 10.1021/acs.jpclett.0c03853.
(73) W. Chu, Q. Zheng, A. V. Akimov, J. Zhao, W. A. Saidi and O. V. Prezhdo, *J. Phys. Chem. Lett.,* 2020, **11**, 10073-10080. DOI: 10.1021/acs.jpclett.0c03080.
(74) A. E. Sifain, L. Wang and O. V. Prezhdo, *J. Chem. Phys.,* 2015, **142**, 224102. DOI: 10.1063/1.4922162

(75) L. Wang, D. Trivedi and O. V. Prezhdo, *J. Chem. Theory Comput.,* 2014, **10**, 3598-3605. DOI: 10.1021/ct5003835.
(76) J. C. Tully, *J. Chem. Phys.,* 1990, **93**, 1061. DOI: 10.1063/1.459170.
(77) P. V. Parandekar and J. C. Tully, *J. Chem. Phys.,* 2005, **122**, 094102. DOI: 10.1063/1.1856460.
(78) A. V. Akimov and O. V. Prezhdo, *J. Phys. Chem. Lett.,* 2013, **4**, 3857-3864. DOI: 10.1021/jz402035z.
(79) A. V. Akimov, R. Long and O. V. Prezhdo, *J. Chem. Phys.,* 2014, **140**, 194107. DOI: 10.1063/1.4875702.
(80) Z. Zhang, W.-H. Fang, M. V. Tokina, R. Long and O. V. Prezhdo, *Nano Lett.,* 2018, **18**, 2459-2466. DOI: 10.1021/acs.nanolett.8b00035.
(81) S. V. Kilina, A. J. Neukirch, B. F. Habenicht, D. S. Kilin and O. V. Prezhdo, *Phys. Rev. Lett.,* 2013, **110**, 180404. DOI: 10.1103/PhysRevLett.110.180404.
(82) A. Giri, J. T. Gaskins, B. M. Foley, R. Cheaito and P. E. Hopkins, *Journal of Applied Physics,* 2015, **117,** DOI: 10.1063/1.4906553.
(83) D. H. Olson, M. G. Sales, J. A. Tomko, T. Lu, O. V. Prezhdo, S. J. McDonnell and P. E. Hopkins, *Appl. Phys. Lett.,* 2021, **118,** DOI: 10.1063/5.0046566.